# EPR and ENDOR Studies of Single Crystals of α-Glycine X-ray Irradiated at 295 K

**Audun Sanderud and Einar Sagstuen***

*Department of Physics, University of Oslo, P.O. Box 1048 Blindern, N-0316 Oslo, Norway*

*Received: July 9, 1998; In Final Form: August 31, 1998*

Single crystals of the amino acid α-glycine $H_3^+N-CH_2-COO^-$ were X-ray irradiated at 280 K and studied at 295 K and at 100 K using EPR, ENDOR, and EIE techniques. Five radicals were detected and characterized. Two of these are well known from previous studies, the oxidation product $H_3^+N-\dot{C}H-COO^-$ (radical I) and the reduction product $\dot{C}H_2-COO^-$ (radical II). It is shown that at 295 K the ENDOR and EIE spectra from radical I are characteristic of efficient $W_{1x}$ cross relaxation induced by rapid rotation of the amino group. This allows for the determination of the absolute signs of the hyperfine coupling constants of radical I. The other three radicals are two geometrical conformations of the product $H_2N-\dot{C}H-COOH$ (radicals III and IV) and a species suggested to be the dimer product $H_3^+N-CH_2-CO-\dot{C}H-COO^-$ (radical V). Radical III exhibits spectral parameters related to those previously reported by M. Brustolon et al. (*J. Phys. Chem.* **1997**, *101*, 4887). However, on the basis of our analysis of ENDOR and EIE spectra from normal as well as from partially deuterated crystals, the structural assignment for radical III is different from that suggested by these authors. A comparison with a new radical species recently observed and characterized in irradiated crystals of the amino acid L-α-alanine indicates that the new alanine radical and radical III presented here have similar structures. A review of the mechanistic aspects of radical formation in glycine is given, and the newly detected species (radicals III−V) are tentatively fitted into this scheme.

## 1. Introduction

A large number of reports on free radical production in single crystals of the simplest amino acid α-glycine, $NH_3^+CH_2COO^-$, after exposure to ionizing radiation at room temperature, have appeared in the literature.[1,2,3] As early as in 1964, from Electron Paramagnetic Resonance (EPR) studies of α-glycine crystals X-ray and $\gamma$-ray irradiated at room temperature, Morton[1] determined the structure of two radicals. One was the oxidation product[4] $NH_3^+\dot{C}HCOO^-$ (radical I), formed by net hydrogen abstraction from the central carbon atom, and the second was a reduction product[4] $\dot{C}H_2COO^-$ (radical II, although most probably protonated at a carboxylic oxygen) formed by net deamination.

Collins and Whiffen[2] determined the hyperfine coupling (hfc) tensors of radical I from electron−nuclear double resonance (ENDOR) studies at room temperature and at 77 K, using crystals irradiated at room temperature. These authors observed that the amino group of radical I is rotating freely at room temperature and that the couplings to the three amino protons are rotationally averaged. At 77 K, however, the amino group is locked into one position and thus three different amino proton hfc tensors are observed. From ENDOR studies at low temperature, the hfc tensors of the two methylene protons of radical II were determined by Teslenko et al.[5] At room temperature the two protons are equivalent due to motional averaging.

The low-temperature irradiation and EPR/ENDOR analysis of glycine crystals have shown that even for this simple amino acid, the radiation chemistry is complex.[6] Iwasaki and coworkers[7−9] discussed the radicals formed after 4 K irradiation and measurement, and several other authors[6,10−12] have analyzed sequences of reactions taking place and products formed from the initially formed anion and cation radical species. The bulk of experimental data may suggest possible schemes of radical reactions, but even after many years of intensive studies, pieces still are missing in the complex puzzle of mechanistically connecting the various radical products stabilized at different temperatures.

Very recently, Brustolon et al.[13] reported the detection of a third radical in glycine after room-temperature irradiation. This species, radical III, was suggested to be the amino deprotonated decarboxylation product $NH_2\dot{C}H_2$, a product not previously identified with certainty in glycine crystals. That paper appeared while detailed EPR/ENDOR studies of X-ray irradiated glycine crystals were performed in our laboratories as well. The resonance due to this third radical species was also observed in our work. However, our measurements including ENDOR-induced EPR (EIE) have led us to a different structural assignment for this radical. In addition, two additional radical species, not previously observed, have been analyzed and characterized in the present work.

Together with the recent EPR and ENDOR results from crystals of the amino acid *l*-α-alanine[14] the present results shed further light on the secondary radiation chemistry of simple amino acids.

## 2. Experimental Section

Single crystals of α-glycine (Sigma Chemical Co.) were

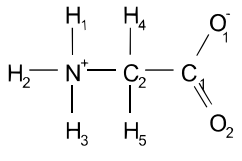


α-Glycine

grown from aqueous solutions saturated at room temperature

* To whom all correspondence should be addressed.

10.1021/jp982932j CCC: $15.00 
Published on Web 10/26/1998

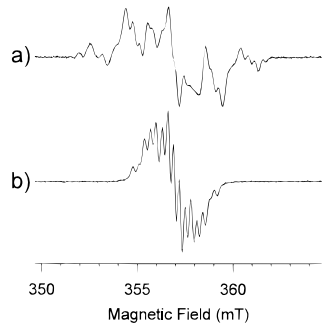


**Figure 1.** First-derivative EPR spectra (centered at $g_e = 2.0023$) of α-glycine single crystals, X-ray irradiated at 280 K and measured at room temperature. Spectrum a is recorded using crystals grown from water, while spectrum b is recorded using a partly deuterated crystal. The spectra are measured with the external magnetic field along ⟨*a**⟩.

by slow cooling. Partially deuterated samples were similarly prepared by repeated recrystallization from 99.8 g/100 g purity deuterium oxide solutions (Sigma Chemical Co.). Only the amino group protons are expected to be exchanged with deuterons by the procedure used. The crystal structure of α-glycine has been solved by Jönsson and Kvick.[15] The unit cell is monoclinic with space group $P2_1/c$ and $Z = 4$.

The crystals were irradiated at 280 K using X-rays from a Phillips tungsten target tube operated at 60 kV and 50 mA. Each sample received a total dose of 50 kGy at a rate of about 30 kGy/h. The crystals were aligned along each crystallographic axis using a Weissenberg X-ray diffraction camera and subsequently transferred to the quartz sample holder of an EPR goniometer without loss of rotation axis alignment. The tensor parameters are related to the orthogonal axis system ⟨*a***bc*⟩. First-derivative EPR and ENDOR spectra, and the ENDOR-induced EPR (EIE) spectra at room temperature and at 100 K, were collected at X-band microwave frequencies. The spectrometer used was a Bruker ER 200 D-SRC spectrometer with an EN 200 ENDOR unit equipped with a 100 W ENI rf amplifier. The data were recorded at 5° intervals of rotation through each plane of rotation. In addition, an experiment using a rotation axis skewed with respect to the crystallographic axes was performed to resolve the so-called Schonland ambiguity.[16]

The proton hfc tensors were determined using the program NQENDFIT.[17]

## 3. Results

**3.1. EPR.** The EPR spectra from α-glycine at room temperature are well-known from previous studies. Some selected spectra are shown in Figure 1. The magnetic field is directed along ⟨*a**⟩. The spectrum in Figure 1a is from the undeuterated crystal while the spectrum in Figure 1b is obtained using a partially deuterated crystal. The difference between the two spectra is dramatic, indicating that some of the major couplings are due to interaction of the unpaired electron with the amino group protons.

Since the EPR spectra contain contributions from several radicals, they were difficult to analyze. The ENDOR/EIE analysis, however, gave good results and thus radical structures were determined without further use of the EPR data other than establishing that the various resonances exhibit only small *g*-factor variations.

**3.2. ENDOR/EIE.** Figure 2 shows ENDOR spectra obtained with the magnetic field along ⟨*b*⟩ for the nondeuterated crystals at room temperature (Figure 2a) and at 100 K (Figure 2b). On the spectrum in Figure 2a, the high-frequency branch ENDOR

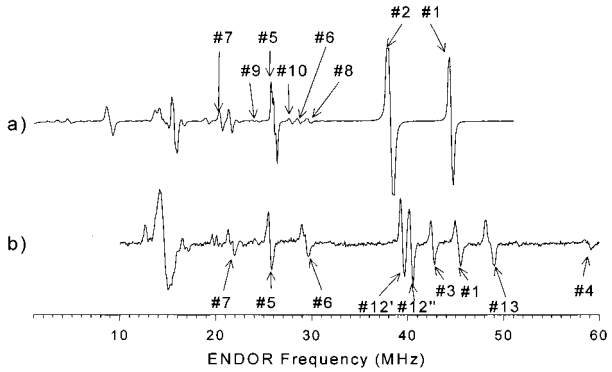


**Figure 2.** First-derivative ENDOR spectra of α-glycine single crystals, X-ray irradiated at 280. The spectra are measured with the external magnetic field along ⟨*b*⟩. Spectrum a is measured at room temperature, while b is measured at 100 K, using crystals grown from water. Most of the ENDOR transitions discussed in this paper are indicated by numbers.

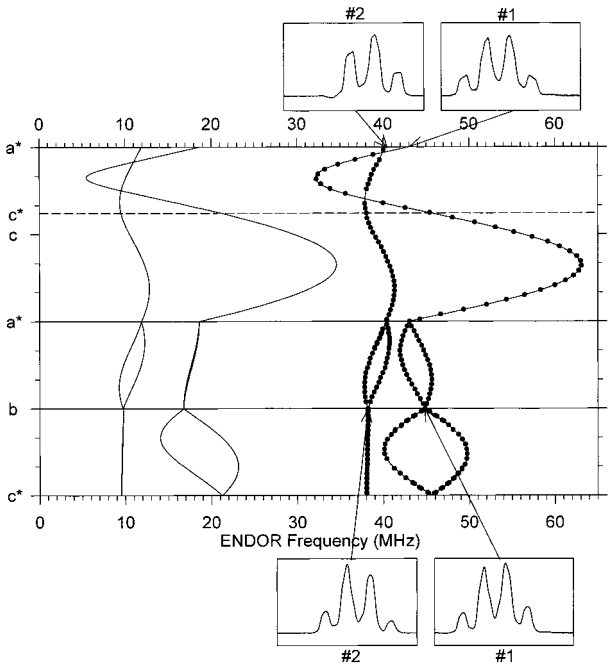


**Figure 3.** Angular variations of the ENDOR transitions from the proton couplings 1 and 2 of radical I in α-glycine single crystals X-ray irradiated at 280 K and measured at room temperature. The solid curves are calculated from the hfc tensors listed in Table 1. The EIE spectra (sweep width 11.8 mT, centered at $g_e = 2.0023$) connecting these couplings to one radical are shown.

transition lines which were used to determine the hyperfine coupling (hfc) tensors are marked as **#1**, **#2**, and **#5**−**#10** (**#11** is overlapping with **#2**). On the low-temperature spectrum in Figure 2b, two additional lines associated with radical I are marked as **#3** and **#4**, whereas two other lines that are associated with radical II are marked as **#12** and **#13**. These lines of radical II have not been further analyzed in this work.

It thus appears that the room-temperature ENDOR spectra reveal nine different proton hfc's which could be followed through all three planes of rotation. The angular variations of these couplings are shown in Figures 3, 7, 10, and 11. From these data, nine proton hfc tensors were determined. In addition, two hfc tensors (**#3**, and **#4**) were determined from the low-temperature ENDOR studies. The corresponding angular variation diagrams are shown in Figure 5.

Hyperfine coupling tensors based on data from rotations around the crystallographic axes leave an ambiguity in the signs

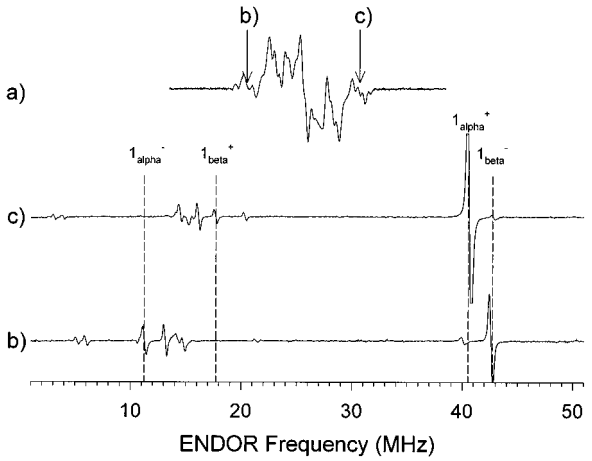


**Figure 4.** ENDOR spectra recorded off the low-field EPR line position b and the high-field EPR line position c, with the crystal oriented along ⟨*a**⟩. In the former case, the high-frequency ENDOR due to interaction with the α-proton of radical I together with the low-frequency branch of the ENDOR due to interaction with the three amino protons are dominating the spectrum. This behavior is reversed in the ENDOR spectrum obtained off position c.

of the off-diagonal tensor elements. Schonland[16] pointed out that this ambiguity might be resolved by investigating a plane of data using a skewed axis of rotation. This method has been used in this work (rotation axis polar angles $\theta = 50°$ $\phi = 90°$) for tensors **#1**, **#5**, **#6**, **#7**, **#8**, and **#11**. For the other tensors, the differences between the two tensor alternatives were small and indirect arguments were used to settle on those chosen.

EIE was used to assign the ENDOR lines in Figure 2 to five different radicals. In the following sections, only short descriptions are given for the well-known radicals I and II, highlighting some details on new observations with regard to effects of cross relaxation on the ENDOR lines due to radical I. The main emphasis is put on the data leading to the assignment of the three new radical structures in glycine crystals at room temperature.

**3.3. Radical I.** Radical I is the major species formed at room temperature. The EPR spectrum in Figure 1a is mostly due to this radical. At room-temperature two ENDOR resonance lines (Figure 2a, **#1** and **#2**) were assigned to this radical by EIE. This is shown in more detail in Figure 3.

A striking feature of these EIE spectra is their asymmetry. A very similar situation was recently encountered in the case of EIE spectra from the dominating radical in alanine crystals.[14] Here, it was shown that this effect is due to efficient $W_{1x}$ electron−nuclear flip−flop cross relaxation induced by rapid methyl group rotation.[18] As also shown for alanine, this behavior allows for the determination of the absolute signs of the coupling constants from regular ENDOR spectra. In glycine, the rotating amino group may provide a similar efficient $W_{1x}$ relaxation mechanism and thus asymmetric EIE spectra. Figure 4 shows ENDOR spectra recorded off the low-field EPR line position b and the high-field EPR line position c, with the crystal oriented along ⟨*a**⟩. In the former case, the intensity of the high-frequency ENDOR line (designated $1_{alpha}^{+}$) due to interaction with the α-proton of radical I dominates over that of the low-frequency branch (designated $1_{alpha}^{-}$). Similarly, the intensity of the low-frequency branch of the ENDOR due to the $\beta$-interaction with the three amino protons (designated $1_{beta}^{+}$) dominates over that of the high-frequency branch (designated $1_{beta}^{-}$). This behavior is reversed in the ENDOR spectrum obtained off position c. This shows,[14] as expected, that the two

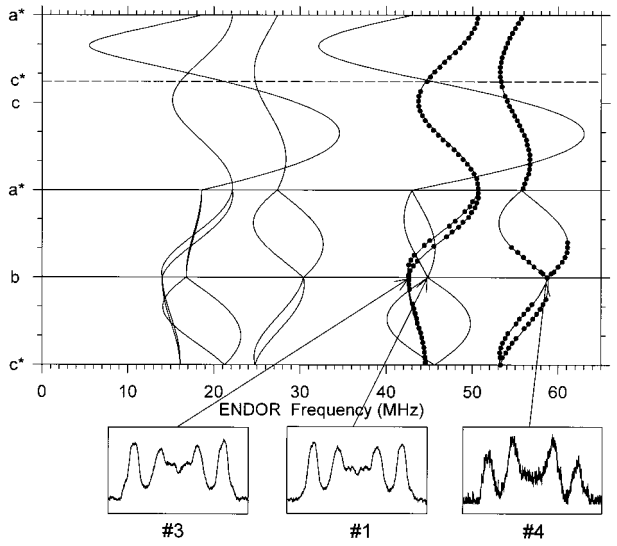


**Figure 5.** Angular variations of the ENDOR transitions from the proton couplings 3 and 4 of radical I in α-glycine single crystals X-ray irradiated at 280 K and measured 100 K. The solid curves are calculated from the hfc tensors listed in Table 1. The EIE spectra (sweep width 11.8 mT, centered at $g_e = 2.0023$) connect these couplings to coupling 1 and thereby to radical I. Coupling 2 is no longer present at 100 K.

interactions have different signs and further that the α-proton coupling is negative and the amino proton coupling is positive.[14,19]

Figure 5 shows that at 100 K, the EIE spectrum off the ENDOR line **#1** was different but the ENDOR line retained its position. The EIE spectra obtained at this temperature were symmetrical indicating that the $W_{1x}$ relaxation rate enhancing effect of the rotating amino group now had disappeared. This conclusion is corroborated by the observation that line **#2** (at room temperature due to the rotating amino group) had disappeared and two new lines (**#3** and **#4**) had grown in which were assigned to radical I by virtue of their EIE spectra (Figure 5). These two couplings are due to two of the three locked-in amino protons, as shown by previous authors.[2] The third amino−proton coupling is very small[2,3] and could in the present work not be distinguished from the plethora of ENDOR lines in the region near the free proton frequency (about 14.6 MHz). The hfc tensors for the four couplings **#1**−**#4** are given in Table 1 and agree excellently with those determined by previous authors.[2,3]

**3.4. Radical II.** As shown in Figure 2, two new ENDOR lines (**#12** and **#13**) were observed at 100 K, at positions coincident with those determined for the two α-protons of radical II by Teslenko et al.[5] Figure 6 shows EIE from these ENDOR lines with the external magnetic field along ⟨*b*⟩. The EIE appear as a triplet resonance, as expected for radical II at this orientation.[5] The two lines denoted **#12′** and **#12″** are due to two slightly different conformations of radical II (similarly, line **#13** is also broadened, at other orientations split, for the same reason). The hfc tensors of these α-proton interactions were not re-evaluated.

**3.5. Radical III.** Figure 7 shows the ENDOR line variation for the three proton hyperfine couplings associated with radical III. The hfc tensors (**#5**−**#7**) were obtained and are presented in Table 2. All three hfc tensors were present upon observation at 100 K.

Couplings **#6** and **#7** are due to easily exchangeable protons as deduced from their absence in the ENDOR spectra from the partially deuterated samples. Figure 8 shows EIE spectra obtained with the external magnetic field oriented along ⟨*c*⟩ .

**TABLE 1: Hyperfine Coupling Tensors for Radical I in Single Crystals of α-Glycine X-ray Irradiated at 280 K.[a] Tensors #1 and #2 Are from Data Obtained at Room Temperature, while Tensor #3 and #4 Are from Measurements at 100 K**

| | principal values (MHz) | | | eigenvectors | | |
|---|---|---|---|---|---|---|
| tensor | *A* | $a_{iso}$ | *B* | **a*** | **b** | **c** |
| | −31.78 | | 31.94 | 0.797 | −0.301 | 0.524 |
| **#1** | −61.87 | −63.72 | 1.85 | 0.330 | 0.943 | 0.040 |
| | −97.52 | | −33.80 | −0.507 | 0.141 | 0.851 |
| | 54.04 | | 4.97 | 0.807 | −0.297 | −0.511 |
| **#2** | 47.02 | 49.07 | −2.05 | 0.222 | −0.649 | 0.727 |
| | 46.14 | | −2.93 | 0.548 | 0.700 | 0.458 |
| | 73.57 | | 10.66 | 0.820 | −0.100 | −0.563 |
| **#3** | 58.84 | 62.91 | −4.07 | 0.542 | −0.182 | 0.821 |
| | 56.31 | | −6.60 | 0.184 | 0.978 | 0.095 |
| | 93.70 | | 10.65 | −0.598 | 0.794 | 0.111 |
| **#4** | 78.25 | 83.05 | −4.80 | 0.757 | 0.605 | −0.247 |
| | 77.19 | | −5.86 | 0.264 | 0.064 | 0.963 |

[a] The errors involved in the principal values and the eigenvectors are about ±0.05 MHz and ±3°, respectively.

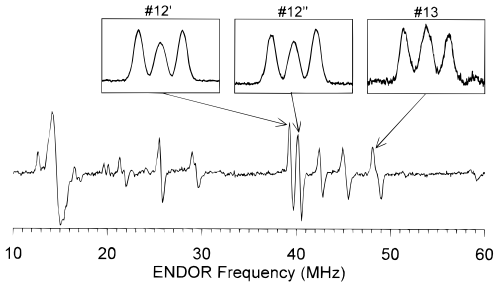


**Figure 6.** First-derivative ENDOR spectra of α-glycine single crystals, X-ray irradiated at 280 K, measured at 100 K. The spectra are obtained with the external magnetic field along ⟨*b*⟩. The EIE spectra (sweep width 11.8 mT, centered at $g_c = 2.0023$) points to three lines associated with radical II.

At this orientation the splitting from coupling **#6** is 0.16 mT only (see Figure 7) and under any circumstances not observable in the EPR or EIE spectra. Furthermore, an assumed nitrogen hyperfine interaction (see below) is very close to zero at this orientation. The two other proton couplings, **#5** and **#7**, are quite similar at this orientation, about 1.3 mT and 1.1 mT, respectively. The EIE spectra in Figures 8a and b, recorded off ENDOR lines 5 and 7, respectively, show that both coupling **#5** and **#7** contributes to the EIE spectra yielding a triplet pattern. The EIE spectrum (at the same orientation as above) shown in Figure 8c is obtained off coupling **#5** using a partially deuterated crystal and shows that only coupling **#5** is present. This proves that coupling **#7** is due to an exchangeable proton. As mentioned above, the full analysis of deuterated crystals shows that this also is the case for coupling **#6**.

As demonstrated in Figure 7, the EIE spectra recorded along ⟨*a**⟩ exhibit a spectral width of about 3.8 mT. The three proton coupling values at this orientation are 0.8 mT (coupling **#5**), 1.1 mT (**#6**), and 0.4 mT (**#7**), which gives a total spectral extent of 2.3 mT only. To account for this EIE spectrum, as well as for the width of the EIE spectra measured at other orientations, it was necessary to assume an additional coupling to a nitrogen nucleus. The details of how this $^{14}$N hfc tensor is estimated are given in section 4.

**3.6. Radical IV.** Figure 10 shows the ENDOR line variation for the three proton hyperfine couplings associated with radical IV. The hfc tensors (**#8**, **#9**, and **#10**) were obtained and are presented in Table 3. All three hfc's were present by observation at 100 K. Couplings **#9** and **#10** disappear in partially deuterated crystals and are therefore associated with protons easily exchanged with deuterium.

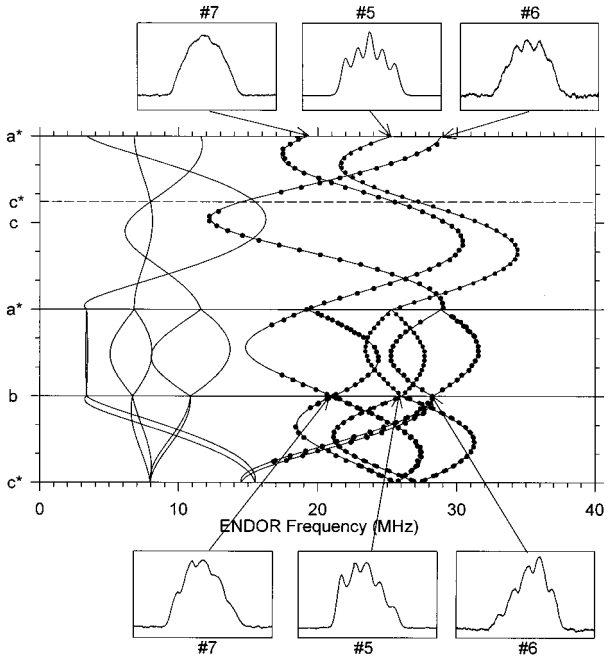


**Figure 7.** Angular variations of the ENDOR transitions from the proton couplings 5−7 of radical III in α-glycine single crystals X-ray irradiated at 280 K and measured at room temperature. The solid curves are calculated from the hfc tensors listed in Table 2. The EIE spectra (sweep width 11.8 mT, centered at $g_e = 2.0023$) connect these couplings to one radical.

**TABLE 2: Hyperfine Coupling Tensors for Radical III in Single Crystals of α-Glycine X-ray Irradiated at 280 K[a]**

| | principal values (MHz) | | | eigenvectors | | |
|---|---|---|---|---|---|---|
| tensor | *A* | $a_{iso}$ | *B* | **a*** | **b** | **c** |
| | −6.85 | | 17.77 | 0.673 | −0.546 | 0.499 |
| **#5** | −26.16 | −24.62 | −1.54 | 0.624 | 0.781 | 0.014 |
| | −40.84 | | −16.22 | −0.397 | 0.302 | 0.866 |
| | 4.75 | | 21.62 | 0.064 | −0.059 | 0.996 |
| **#6** | −21.24 | −16.87 | −4.37 | 0.673 | 0.739 | 0.000 |
| | −34.12 | | −17.25 | 0.737 | −0.671 | −0.087 |
| | 4.94 | | 20.40 | 0.750 | −0.586 | 0.306 |
| **#7** | −19.45 | −15.46 | −3.99 | 0.594 | 0.801 | 0.079 |
| | −31.88 | | −16.42 | −0.291 | 0.122 | 0.949 |

[a] The errors involved in the principal values and the eigenvectors are about ±0.05 MHz and ±3°, respectively.

These three proton hfc tensors exhibit principal values quite similar to those obtained for radical III, but with slightly different eigenvectors. Also for this radical species the EIE spectra were too wide to be accounted for by the three proton couplings alone, and an additional interaction with nitrogen is postulated (see below).

**3.7. Radical V.** Figure 11 shows the EIE spectrum obtained off the ENDOR line from the last of the room temperature hyperfine coupling tensors, **#11**. Surprisingly, the spectrum exhibits a simple doublet only, the splitting of which agrees with the coupling from tensor **#11** at this orientation. Thus, this is the only major coupling associated with radical V. It was difficult to follow the ENDOR line through all the three planes of rotation. However, also in the skew plane the coupling was clearly observable and was used to verify the assignments made from the other rotation planes. The final hfc tensor obtained is presented in Table 4.

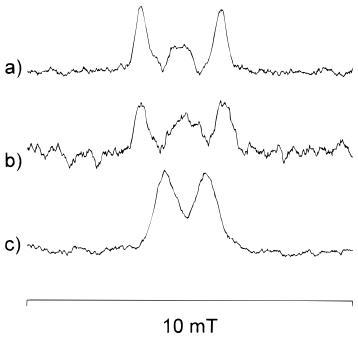


**Figure 8.** EIE spectra (centered at $g_e = 2.0023$) of α-glycine single crystals, X-ray irradiated at 280 K and measured at room temperature. The spectra are recorded with the external magnetic field oriented along ⟨*c*⟩, where the splittings from coupling 6 and the nitrogen coupling are close to zero, while the two other proton couplings, 5 and 7, are approximately equivalent. Spectrum a and c is obtained with the ENDOR frequency locked to the high-frequency ENDOR transition of coupling 5. Spectrum c is recorded using a deuterated crystal and only the splitting from coupling 5 is present. Spectrum a is from an undeuterated crystal and the two couplings 5 and 7 yield a triplet. Spectrum b is with the ENDOR frequency locked to the high-frequency ENDOR transition of coupling 7.

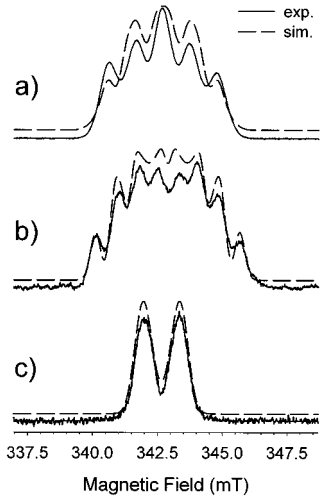


**Figure 9.** The results of simulations of the EIE spectra (sweep width 11.8 mT, centered at $g_e = 2.0023$) from (a) radical III, (b) radical IV, and (c) radical V. All experimental spectra are obtained with the magnetic field along ⟨*a**⟩ and at 280 K.

## 4. Discussion of Radical Structures

**4.1. Radical I.** The four tensors associated with radical I,

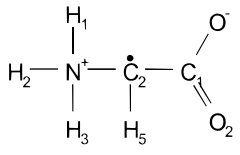


*Radical I*

**#1**−**4**, given in Table 1, are all very similar to those obtained by Collins and Whiffen[2] and by Hedberg and Ehrenberg.[3] These authors in addition determined a fifth coupling, the third low-temperature amino *β*-proton tensor, which is far smaller than the other two. The very good agreement obtained with two other, independent studies also lend credibility to the data analysis and radical assignment to follow in the next paragraphs.

**4.2. Radical III.** From the EIE experiments, three (**#5**−**#7**) of the ENDOR determined hfc tensors were associated with Radical III. As shown in Figure 8, coupling **#5** has been proven

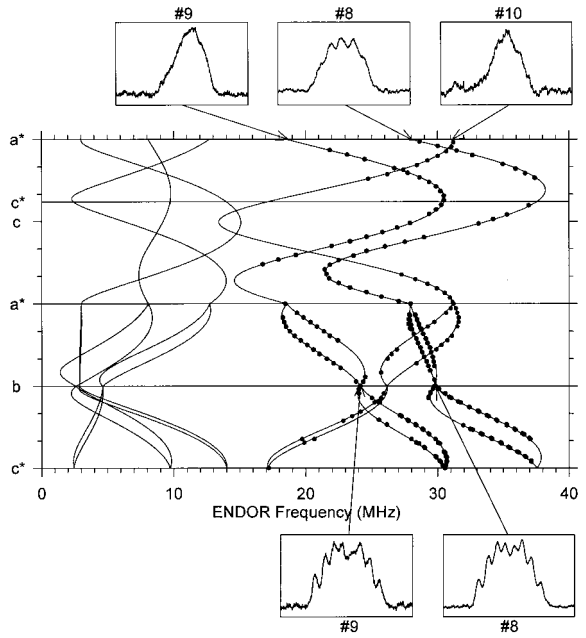


**Figure 10.** Angular variations of the ENDOR transitions from the proton couplings 8−10 of radical IV in α-glycine single crystals X-ray irradiated at 280 K and measured at room temperature. The solid curves are calculated from the hfc tensors listed in Table 3. The EIE spectra (sweep width 11.8 mT, centered at $g_e = 2.0023$) connect these couplings to one radical.

**TABLE 3: Hyperfine Coupling Tensors for Radical IV in Single Crystals of α-Glycine X-Irradiated at 280 K[a]**

| | principal values (MHz) | | | eigenvectors | | |
|---|---|---|---|---|---|---|
| tensor | *A* | $a_{iso}$ | *B* | **a*** | **b** | **c** |
| | −12.67 | | 17.48 | 0.794 | −0.208 | 0.572 |
| **#8** | −30.38 | −30.15 | −0.19 | 0.263 | 0.965 | −0.014 |
| | −47.39 | | −17.24 | −0.549 | 0.161 | 0.820 |
| | 1.55 | | 18.34 | 0.871 | −0.233 | 0.433 |
| **#9** | −19.73 | −16.79 | −2.94 | 0.276 | 0.960 | −0.039 |
| | −32.18 | | −15.39 | −0.407 | 0.153 | 0.901 |
| | 2.23 | | 20.28 | 0.013 | −0.031 | 0.999 |
| **#10** | −22.33 | −18.05 | −4.18 | 0.269 | 0.962 | 0.033 |
| | −34.05 | | −16.00 | −0.963 | 0.270 | 0.005 |

[a] The errors involved in the principal values and the eigenvectors are about ±0.05 MHz and ±3°, respectively.

to be due to an unexchangeable proton, whereas couplings **#6** and **#7** are due to exchangeable protons. Couplings **#6** and **#7** are similar in magnitude and exhibit principal values for the dipolar coupling tensors that indicate both to be bonded to a nitrogen atom.[20,21] These exchangeable protons must be two of the protons of the amino group. The third coupling must be due to one of the carbon bonded protons, which are the only nonexchangeable protons in this molecule.

In addition the EIE spectra reveal that at least one more coupling contributes to the resonance of radical III. Since couplings to two of the amino group protons apparently are present, a $^{14}$N hfc should be expected as well. Nitrogen hyperfine couplings are often very difficult to observe by conventional ENDOR spectroscopy. However, on the basis of an estimate of the nitrogen spin density, an approximate $^{14}$N hfc tensor will be calculated below.

All the three proton hfc tensors are of the α-type. The eigenvectors for the intermediate principal values of the two nitrogen-bonded α-tensors (**#6** and **#7**), which represent the direction of the lone electron orbital (LEO),[22] are almost parallel (angle of deviation is 7.4°). Furthermore, the angle between

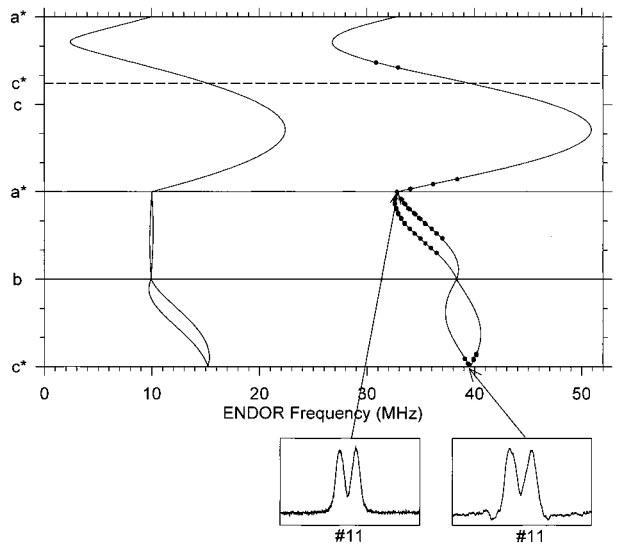


**Figure 11.** Angular variations of the ENDOR transitions from the proton coupling 11 of radical V in α-glycine single crystals X-ray irradiated at 280 K and measured at room temperature. The solid curves are calculated from the hfc tensor listed in Table 4. The EIE spectra (sweep width 11.8 mT, centered at $g_e = 2.0023$) are associated with this coupling.

**TABLE 4: Hyperfine Coupling Tensors for Radical V in Single Crystals of α-Glycine X-ray Irradiated at 280 K[a]**

| | principal values (MHz) | | | eigenvectors | | |
|---|---|---|---|---|---|---|
| tensor | *A* | $a_{iso}$ | *B* | **a*** | **b** | **c** |
| | −24.26 | | 23.73 | 0.899 | 0.005 | 0.438 |
| **#11** | −46.70 | −47.99 | 1.29 | −0.069 | 0.989 | 0.131 |
| | −73.02 | | −25.03 | −0.432 | −0.148 | 0.889 |

[a] The errors involved in the principal values and the eigenvectors are about ±0.05 MHz and ±3°, respectively.

the LEO directions of these two tensors (**#6** and **#7**) and the crystallographic N−C2 bond are 100.5° and 93.3°, respectively. This suggests that the amino nitrogen exhibits a configuration which is near (but not completely, see below) $sp^2$ in the radical and thus that the third N-bonded proton must have been abstracted.

The $2p^\pi$ spin density of a $sp^2$-hybridized nitrogen atom usually may be estimated from the N−H α-tensor principal values. Using the isotropic value of the couplings and $Q^H_{NH} = -81$ MHz[21] in the McConnell relation[23] a spin density of about 0.21 is obtained. However, the >N−H dipolar coupling tensor seems to be larger than that expected for a $2p^\pi$ spin density of only 0.21. Thus, for an isolated N−H fragment calculations[20,43] (unit spin) yields dipolar coupling principal values of (69.44, −14.84, −54.6) MHz. Scaling down to those observed for **#6** and **#7** indicates nitrogen 2p spin densities of the order of 0.30. This discrepancy is often ascribed to bending at the radical center leading to reduced (that is, larger positive) isotropic H(N) couplings.[25]

The angle between the eigenvector of the smallest principal value of tensor **#6** and the crystallographic N−H1 bond direction is only 2.4°, and for tensor **#7** the corresponding angles with the crystallographic N−H2 and N−H3 bond directions are 55.4° and 51.4°, respectively. This indicates that coupling **#6** is due to an interaction with the H1-atom, while coupling **#7** is to one of the H2- or H3-atoms which has experienced some reorientation upon amino deprotonation.

Coupling **#5** must be due to an interaction with one of the H-atoms bonded to the C2-atom. The extent of rehybridization of the C2-atom toward a planar $sp^2$ configuration can be examined by comparing two methods for finding the $2p^\pi$ spin density at C2 from the α-coupling tensor **#5**. One method consists of using the isotropic value, $a_{iso} = -24.62$ MHz, in the McConnell relation[23] with $Q^H_{CH} = -73.4$ MHz[26] for a planar $sp^2$ configuration.[27] This gave $\rho^\pi_{iso} = 0.335$. The other method consists of using the dipolar part of the α-coupling tensor **#5** in the Gordy−Bernhard method,[28] giving $\rho^\pi_{dip} = 0.459$ with $Q^{dip}_z = 38.7$ MHz. The discrepancy between these two values is again ascribed to a nonplanarity around the radical center so that the carbon lone electron orbital (LEO) exhibits a significant degree of 2s character. Sørnes et al.[17] showed that, under similar circumstances, the (orthogonal) hfc principal axis system is determined by the direction of the LEO and the external bisector of the $N-C_2-C_1$ fragment. Thus, the eigenvector for the minimum principal value will not represent the true C−H bond direction, but the projection of this into the $N-C_2-C_1$ plane. The data in Table 2 shows that the angle between this *apparent* C−H bond direction and the crystallographic C2−N bond direction is 121.3°, while that with the crystallographic C2−C1−bond it is 126.9°. The angle between the N−C2 and the C1−C2 bonds is 111.8°. The sum of these three angles is 360.0°. This indicates that one of the two H-atoms H4 or H5 is lost upon radical formation. The angles between the LEO direction of tensor 5 and the crystallographic C2−H4 and C2−H5 bonds are 54.3° and 54.4°. Our data can hence not distinguish which of these protons have been abstracted. These considerations all lead to the conclusion that radical III is a formed by removing one of the H atoms bonded to C3 and one of the amino group protons, and has the structure as shown below (protonation at the carboxyl group is assumed

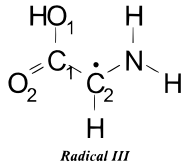


*Radical III*

based on data from aqueous solution, see below).

As discussed above, neither the $C_2$ atom nor the nitrogen atom has attained completely planar $sp^2$ configurations. However, by comparing the directions, of the three LEO directions it appears that the angle of deviation between **#5** and **#6** is 4.4° and that between **#5** and **#7** is 4.2°. Thus, the nitrogen and the $C_2$ LEO directions are virtually coaxial.

The 2p orbital spin density at the N-atom was estimated above to be of the order of 0.30 from the dipolar coupling of the two H(N) α-coupling tensors. This spin density can be used for a rough first estimate the expected nitrogen hfc tensor. Nitrogen centered couplings typically exhibit axially symmetric hfc tensors with principal values of the form $(3a_d, 0, 0)$ where $a_{iso} \cong a_d$, and with the symmetry direction along the LEO.[29] Here, $a_d = (2/5)g\beta g_N\beta_N\langle r^{-3}\rangle$ which for unit spin is 47.8 MHz.[30] With a 2p spin density of about 0.3 the principal values of (43, 0, 0) MHz are obtained. With the magnetic field along $\langle a^*\rangle$ this yields a nitrogen splitting of about 0.7 mT which added to the other couplings gives a total spectra width of 3.7 mT. Considering the approximate nature of this analysis this is a reasonable agreement with the experimental value of 3.8 mT.

Figure 9a shows the results of a simulation of the EIE spectrum from radical III with the magnetic field along $\langle a^*\rangle$ (see also Figure 7). In addition to the hfc tensors listed in Table 2, trial and error indicated that a nitrogen hfc tensor with principal values (51.8, 5.5, 0.0) MHz (using the eigenvector

basis of tensor 6) was necessary to best fit (stipled spectrum) the experimental (fully drawn) spectrum.

The data for radical III as given in Table 2, together with the estimated nitrogen coupling above, agree well with those obtained from aqueous solution[31] provided the radical is protonated at the carboxyl group. Only the magnitude of the isotropic value of coupling **#5** is somewhat smaller than that previously measured (24.6 MHz vs 33.04 MHz,[31] respectively). This discrepancy is most probably due to that the radical structure is more fully structurally relaxed in solution so that there is negligible bending at $C_2$. This will increase the magnitude of the isotropic splitting constant, and using $Q = -73.4$[26] MHz in the McConnell relation,[23] a spin density of 0.452 is obtained from the aqueous solution data. This is almost identical to that obtained from the dipolar coupling tensor in the present work, 0.459 (see above).

It is interesting to note that the angle between the LEO-direction of tensor **#5** and the normal vector to the carboxyl group is 24.2°. This suggests that the $N-C_2-C_1$ plane is twisted about 24° around the $C_1-C_2$ bond with respect to the $O_1-C_1-O_2$ plane. The twist between the two planes $N-C_2-C_1$ and $O_1-C_1-O_2$ from the crystallographic data is about 18.5°.

**4.3. Radical IV.** Figure 10 shows the complete set of ENDOR data obtained from radical IV. Three couplings (**#8**, **#9**, and **#10**) were assigned to this radical from their EIE spectra. Coupling **#8** is due to a nonexchangeable proton, whereas **#9** and **#10** disappear in partially deuterated crystals. The hfc tensors arrived at are given in Table 3.

The two exchangeable couplings are very similar and typical for α-NH fragments. The two eigenvectors for the intermediate principal values (expected direction of the LEO) make an angle of only 2.5°. Similarly, the LEO direction of coupling **#8** is nearly parallel to directions for the couplings of **#9** and **#10** (deviations about 2°), and finally, all three LEO directions are almost parallel with the normal to the $O_1-C_1-O_2$ fragment, the mean angle of deviation being of the order of 5°. Estimating spin densities, the isotropic values of couplings **#9** and **#10** suggest $\rho_N^\pi = 0.21$ and 0.22, respectively. From the dipolar coupling tensors or **#9** and **#10**, the nitrogen 2p spin density is estimated to about 0.28. The isotropic value of coupling **#8** yields a spin density $\rho_{iso}^\pi = 0.41$, whereas the dipolar coupling yield a spin density $\rho_{dip}^\pi = 0.45$. Upon comparison with the corresponding data for radical III, it appears that the bending at the carbon now has almost disappeared whereas that at the nitrogen has been somewhat reduced.

The available experimental data suggest strongly that radical IV exhibit the same structure as radical III (see above). The major difference seems to be the conformation of the radical. Radical III apparently is significantly bent at $C_2$ and at N. In addition the radical plane is twisted about 24° around the $C_2-C_1$ bond with respect to the perpendicular to the $O_1-C_1-O_2$ group. Radical IV seems to be almost planar at $C_2$, exhibits a slightly less bending at the nitrogen atom, and in addition the radical plane is coplanar with the $O_1-C_1-O_2$ group.

As was the case also for radical III, the spectral extent of the EIE spectra in Figure 10 indicates the presence of an additional nitrogen coupling. The magnitude of this coupling is comparable to that for radical III. However, from the spin density estimate above, a slightly smaller maximum value is expected. This is supported by the simulation of the *b*-axis EIE spectrum shown in Figure 9b (fully drawn spectrum, see also Figure 10). For the best-fitting simulation (stipled spectrum), a nitrogen hyperfine coupling of (42.6, 0, 0) MHz was used (eigenvector basis of coupling **#8**) together with the proton hfc tensors given in Table 3.

**4.4. Radical V.** The hyperfine coupling tensor (**#11**) in Table 4 is a typical α-CH coupling tensor. The eigenvectors are nearly coaxial with those for the $C_2-H$ fragment of radicals I and IV, which suggests that the radical is centered at $C_2$, formed by net abstraction of one of the hydrogens from this position. Estimating spin densities, the isotropic value of coupling **#11** yields $\rho_{iso}^\pi = 0.65$, whereas the dipolar coupling yield a spin density $\rho_{dip}^\pi = 0.61$. The reasonable agreement between the two values suggests that the $>C_2-H$ fragment is almost planar also in this radical.

The low spin density of about 0.65 suggests a significant delocalization of the unpaired spin density. Furthermore, the absence of any other resolvable hyperfine interactions shows that nuclei with spin are probably not positioned in α- or *β*-position to $C_2$. In particular, the amino group cannot be present as nearest neighbor to the $C_2$-atom. The unequivocal EIE showing a single proton interaction also shows that a structure exhibiting two α-proton interactions must be dismissed. Figure 9c shows the simulation (stipled curve) of the experimental *a**-axis EIE spectrum (fully drawn curve) using the tensor data in Table 4.

It has not been possible to devise any structure accounting for these features of radical V formed from one single glycine

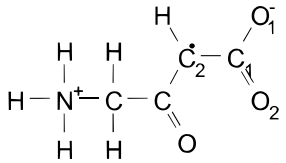


*Radical V*

molecule. The "missing" amino group interactions suggest a dimeric type species. One possibility for a structure accounting for all features of radical V is the structure above, where the carbonyl oxygen may act as a sink for the spin density together with the carboxyl oxygens, the latter to an extent determined by the planarity of the radical fragment. This structure immediately suggests one possible route for its formation. Starting with the deaminated cation $\dot{C}H_2COO^-$, the dimer shown above (radical V) may be envisaged formed by elimination of water between the initial radical product and a neighboring glycine molecule.

## 5. Spin Density Calculations

Using the RHF−INDO/CI LCAO MO-method outlined by Oloff and Hüttermann,[32] the spin density distribution of radicals III/IV was calculated. Starting with standard bond lengths and bonding angles, the geometry was energy optimized using the AM1 package.[33] The energy-optimized structure was virtually completely planar. This energy-optimized structure was then used as input for the RHF−INDO/CI program. The result of this calculation is shown in Table 5.

It is clear that there is a basic agreement between the spin density distribution arrived at by analysis of the experimental data and that obtained from the calculations, thus supporting the radical structure assignment made. Trial calculations showed that quite small deviations from the energy-minimum structure resulted in significant variations in the spin density distribution. The significant amount of spin density at the carbonyl oxygen provides an explanation of the relatively large *g*-value anisotropy of radical III observed using HF EPR spectroscopy by Brustolon et al.[13]

**TABLE 5: RHF/CI INDO−SCF-MO Calculated $2p_z$ Spin Densities for AM1 Energy-Optimized (Vacuum) Geometrical Structures for Radical III in Glycine and Alanine[a]**

| atom | glycine | glycine/exptl radical III/IV[b] | alanine | alanine/exptl conformerI/II[c] |
|---|---|---|---|---|
| N | 0.224 | 0.30 / 0.28 | 0.181 | |
| $C_2$ | 0.473 | 0.46 / 0.45 | 0.453 | 0.44 / 0.38 |
| $O_1$ | 0.253 | | 0.286 | |

[a] $H_2N - \dot{C}_2R$ - $C_1(O_2^-) = O$, glycine; $R = H$; alanine, $R = CH_3$. [b] Present work. [c] Reference 14.

It is interesting to note that, in a recent paper,[14] a radical observed in single crystals of l-α-alanine, X-ray irradiated at room temperature, was suggested to exhibit the same basic structure as that of radicals III and IV, with the exception that the proton bonded to $C_2$ is replaced with a methyl group. Using a procedure similar to that adopted for the glycine radical above, the spin density distribution of the alanine radical was calculated as well. The pertinent results from this calculation are included in Table 5.

## 6. Mechanistic Aspects

In spite of the simplicity of the α-glycine molecule, the literature shows a bewildering number of products formed subsequently to exposure to ionizing radiation. The reduction sequence seems to be best characterized. Following the primary reduction event by capturing an electron, the glycine anion protonates at the carboxy group[7] by proton transfer from a hydrogen-bonded neighboring molecule. This is followed by deamination yielding the $\dot{C}H_2COOH$ radical (A2)[6] which has been suggested to deprotonated (A2′). A major part of the A2 or A2′ radicals transform by H-abstraction from a neighboring molecule[34] into the $NH_3^+CHCOO^-$ product, radical I, above 200 K, but a fraction of the $\dot{C}H_2COO(H)$ species remain stable at room temperature and has been analyzed by various authors.[5,35]

A far more complicated sequence of events seems to take place after electron loss, however. Two species have been suggested, the *σ*-radical $NH_2CH_2COO$ species[8] (K1) by deprotonation from the amino group, and the electronically rearranged nitrogen centered *π*-radical species $NH_2^+CH_2COO^-$ (K2).[8,36] The latter seems to relax slowly into a conformational slightly different product K2′.[8,10] Upon 77 K photolysis using various wavelengths of the light, the products $H\dot{N}CH_2COO^-$ and $NH_3^+\dot{C}H_2$ were detected.[37] Upon thermal annealing from 77 K, Product K2 or K2′ has been suggested to convert directly into $NH_3^+CHCOO^-$ (radical I) by intramolecular hydrogen transfer,[6,38] but several authors also have suggested an alternative decay route, involving decarboxylation of K2 or K2′ as an intermediate step.[10,39] Thermochemical properties of glycine radicals[40] as well as detectable amounts of $CO_2$ upon chemical analysis of stable radiation products may support this suggestion.[4,12,41] It should be noted that Armstrong et al.[40] points out that the radical $NH_2\dot{C}HCOO(H)$ as detected in aqueous solution[31] are expected products from K2 by spontaneous deprotonation.

Radicals III and IV, which in the present paper are suggested to be two conformational isomers of $NH_2\dot{C}HCOOH$, are thus suggested to be formed in the oxidative sequence of reactions by deprotonation from the rearranged, deprotonated cation K2 or K2′, followed by protonation at the carboxyl group. Radical V is, as noted above, most probably formed by a dimerization process involving the deaminated primary species A2 or A2′.

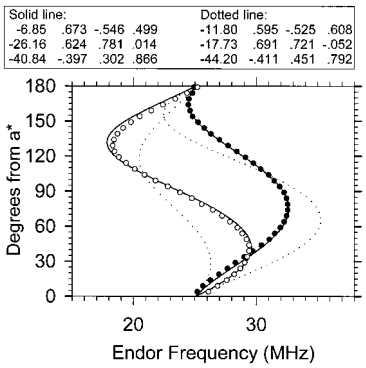


**Figure 12.** The calculated and observed ENDOR line variations through the skewed axis rotation plane (polar angles $\theta$=50°, $\phi$=90°) for coupling 5 in α-glycine single crystals X-ray irradiated at 280 K and measured at room temperature. This plot allows for the determination of the signs of the off-diagonal tensor elements of this coupling. The filled and open circles represent experimental data for the two different molecular sites. The fully drawn curve is calculated from the hfc tensor in Table 2, whereas the dotted line is calculated using a different set of signs of off-diagonal tensor elements. Both hfc tensor alternatives for coupling 5 are given in the figure.

## 7. Concluding Remarks

In a recent paper, Brustolon et al.[13] observed ENDOR due to radical III, but assigned the resonance to a species $NH_2\dot{C}H_2$. Several pieces of evidence were used to argue for this interpretation, although it was noted that the hyperfine coupling constants observed were abnormal for this kind of structure. Two of the coupling tensors agree reasonably well with those obtained in the present work (Table 2, **#6** and **#7**) whereas the third tensor (**#5**) is significantly different. Figure 12 shows experimental ENDOR line positions for coupling **#5** as a function of frequency through a plane of rotation about an axis skewed with respect to the reference coordinate system. The two sites for coupling **#5** are clearly resolved. The fully drawn curve is calculated from the tensor **#5** in Table 2, whereas the dotted line is calculated using a different set of signs of the off-diagonal tensor elements, corresponding to those presented by Brustolon et al.[13] (their coupling denoted *proton 3*). Both tensors are shown in Figure 12. Considering the fit between calculated and observed line positions in Figure 12, it appears that these authors have based their radical assignment on a coupling tensor with incorrect signs of the off-diagonal elements (the second Schonland alternative[16]). This, together with the unequivocal assignment of exchangeable and nonexchangeable protons of this radical, lend strong evidence to the present structural assignment of radical III.

It remains, however, to explain the HYSCORE results of Brustolon et al.[13] (Figure 5 in ref 13). There appears to be weak off-diagonal correlation peaks between tensor **#5** and **#6** (*protons 1* and *3* in ref 13), which may indicate different signs of the splittings.[42] This is not compatible with the proposed structure of radical III in the present paper. However, the same Figure gives no indication of any correlation peaks between *proton 2* and *proton 1* or *3* which would be required for additional confirmation of the conclusion. Due to lack of experimental capabilities we have not been able to pursue this question further. However, from the bulk of available experimental data, it is concluded that radical III exhibit the structure $NH_2\dot{C}HCOOH$.

**Acknowledgment.** Prof. Marina Brustolon is gratefully acknowledged for communicating her results and sending us a preprint of their paper. Prof. William H. Nelson is thanked for his help in doing the AM1 geometry optimizations of alanine

and glycine radicals. We also have enjoyed our discussions and collaboration with Prof. Anders Lund. This work was in part supported by a grant to A.S. from the Norwegian Research Council and exchange visit funding from The Nordic Academy for Advanced Study (NorFA).

## References and Notes

(1) Morton, J. R. *J. Am. Chem. Soc.* **1964**, *86*, 2325.
(2) Collins, M. A.; Whiffen D. H. *Mol. Phys.* **1966,** *10*, 317.
(3) Hedberg, A.; Ehrenberg A. *J. Chem. Phys*. **1968**, *48*, 4822.
(4) Box, H. C. *Radiation Effects: ESR and ENDOR Analysis*; Academic Press: New York, 1977.
(5) Teslenko, V. V.; Gromovoi, Yu. S.; Krivenko, V. G. *Mol. Phys*. **1975**, *30*, 425.
(6) Syutkin, V. M.; Tolkatchev, V. A. *Radiat. Phys. Chem*. **1982**, *20*, 281.
(7) Iwasaki, M.; Muto, H. *J. Chem. Phys.* **1977**, *61*, 5315.
(8) Nunome, K.; Muto, H.; Toriyama, K.; Iwazsaki, M. *J. Chem. Phys.* **1976**, *65*, 3805.
(9) Muto, H.; Iwasaki, M.; Takahashi, Y. *J. Chem. Phys.* **1977**, *66*, 1943.
(10) Sinclair, J. *J. Chem. Phys.* **1971**, *55*, 245.
(11) Deigen, M. F.; Krivenko, V. G.; Pulatova, M. K.; Ruban, M. A.; Teslenko, V. V.; Kayushin, L. P. *Biofizika* **1973**, *18*, 235. Minegishi, A. *J. Phys. Chem.* **1977**, *81*, 1688.
(12) Box, H. C.; Lilga, K. T.; Potienko, G. *Proc. Natl. Acad. Sci. U.S.A.* **1977**, *74*, 2394.
(13) Brustolon, M.; Chis, V.; Maniero, A. L.; Brunel, L.-C. *J. Phys. Chem.* **1997**, *101*, 4887.
(14) Sagstuen, E.; Hole, E. O.; Haugedal, S. R.; Nelson, W. H. *J. Phys. Chem*. **1997**, *101*, 9763.
(15) Jönsson, P.-G.; Kvick, Å. *Acta Crystallogr*. **1971**, *B28*, 1827.
(16) Schonland, D. S. *Proc. Phys. Soc. (London)* **1958**, *73*, 788.
(17) Sørnes A. R.; Sagstuen E. *J. Phys. Chem*. **1995**, *99*, 16857. Sørnes, A. R.; Sagstuen, E.; Lund, A. *J. Phys. Chem*. **1995**, *99*, 16867.
(18) Brustolon, M.; Cassol, T.; Micheletti, L.; Segre, U. *Mol. Phys*. **1986**, *57*, 1005.
(19) Kevan, L.; Kispert, L. D. *Electron Spin Double Resonance Spectroscopy*; John Wiley & Sons: New York, 1976.
(20) Wells, J. H. *J. Chem. Phys.* **1977**, *66*, 632. Sagstuen, E.; Awadelkarim, O.; Lund, A.; Masiakowski, J. *J. Chem. Phys.* **1986**, *85*, 3223.
(21) Nelson, W. H.; Gill, C. *Mol. Phys.* **1978**, *36*, 1779.
(22) McConnell, H. M.; Strathdee, *J. Mol. Phys*. **1959**, *2*, 129.
(23) McConnell, H. M. *J. Chem. Phys.* **1956**, *24*, 764.
(24) Pople, J. A.; Beveridge, D. L. *Approximate Molecular Orbital Theory*; McGraw-Hill Book Company: New York, 1970; p 29.
(25) Chachaty, C.; Forchinoni A.; Virlet J.; Ronfard-Haset J. C. *Chem. Phys. Lett.* **1974**, *29*, 436.
(26) Fessenden, R. W.; Schuler, R. H. *J. Chem. Phys.* **1963**, *39*, 2147.
(27) Dobbs, A. J.; Gilbert, B. C.; Norman, R. O. C. *J. Chem. Soc. A* **1971**, 124.
(28) Gordy, W. *Theory and Applications of Electron Spin Resonance*; John Wiley & Sons: New York, 1980. Bernhard, W. A. *J. Chem. Phys*. **1965**, *24*, 764.
(29) Wertz, J. E.; Bolton, J. R. Electron Spin Resonance: *Elementary Theory and Practical Applications*; Chapman and Hall: New York, 1986.
(30) Morton, J. R.; Rowlands, J. R.; Whiffen, D. H. *Atomic Properties for interpreting ESR data*. BPR 13; National Physics Laboratory: Washington, DC, 1962.
(31) Neta, P.; Fessenden, R. W. *J. Phys. Chem.* **1975**, *75*, 738. Paul, V.-H.; Fisher, H. *Helv. Chim. Acta* **1971**, *54*, 485.
(32) Oloff, H.; Hüttermann J. *J. Magn. Reson*. **1980**, *40*, 414.
(33) Dewar, M. J. S.; Stewart, J. J. P. AMPAC−Austin Method Package QCPE Program. No. 506; Bloomington, IN 47405, 1985.
(34) Syutkin, V. M.; Tolkatchev, V. A. *Chem. Phys. Lett.* **1985**, *122*, 201.
(35) Box, H. C.; Freund, H. G.; Budzinzki, E. E. *J. Am. Chem. Soc.* **1966**, *88*, 658. Morton, J. R. *J. Am. Chem. Soc.* **1966**, *86*, 2325.
(36) Serbodov, M. V.; Symons, M. C. R. *J. Chem. Soc., Perkin Trans. 2*, **1973**, 1808.
(37) Iacona, C.; Michaut, J. P.; Roncin, J. *J. Phys. Chem.* **1977**, *67*, 5658. Ayscough, P. B.; Mack, K. *J. Chem. Soc., Faraday Trans I*. **1972**, *68*, 1139. Bonazzola, L.; Iacona, C, Michaut, J. P.; Roncin, J. *J. Phys. Chem.* **1980**, *73*, 4175.
(38) Smith, C. J.; Poole, C. P.; Farach, H. A. *J. Phys. Chem.* **1981,** *74*, 991.
(39) Sinclair, J. W.; Hanna, M. W. *J. Phys. Chem*. **1967,** *71*, 84. Samskog, P. O.; Gillbro, T.; Nilsson, G. *J. Chem. Phys. Lett*. **1979**, *64*, 162. Samskog, Nilsson, G.; Lund, A. *J. Phys. Chem.* **1980**, *84*, 2819.
(40) Armstrong, D. A.; Rauk, A.; Yu, D. *J. Chem. Soc., Perkin Trans. 2*, **1995**, 553.
(41) Meshitsuka, G.; Shindo, K.; Minegishi, A.; Suguro, H.; Shinozaki, Y. *Bull. Chem. Soc. Jpn.* **1964**, *37*, 928.
(42) Höfer, P.; Grupp, A.; Nebenführ, H.; Mehring, M. *Chem. Phys. Lett*. **1986**, *132*, 279.
(43) Calculated with a nitrogen effective nuclear charge of $Z^* = 3.9$.[24]